NEAR FIELD SMALL EARTHQUAKE LONG PERIOD ARRAY

Charles B. Archambeau, et al

California Institute of Technology

Prepared for:

Air Force Office of Scientific Research
Advanced Research Projects Agency

31 May 1974

California Institute of Technology
Division of Geological and Planetary Sciences
Seismological Laboratory
Pasadena, California 91109

ANNUAL REPORT

1 June 1973 - 31 May 1974

ARPA Order No:	2134
Program Code:	2F10
Contractor:	California Institute of Technology
Effective Date of Contract:	1 June 1973
Contract Expiration Date:	31 May 1974
Amount of Contract:	$73,511
Contract Number:	F44620-72-C-0083, P00001
Principal Investigators:	Charles B. Archambeau Donald V. Helmberger (213) 795-8806
Program Manager:	Lt. Col. Donald W. Klick (202) 694-5275
Title:	Near Field Small Earthquake Long Period Array

Sponsored by
Advanced Research Projects Agency
ARPA Order No. 2134

UNCLASSIFIED

SECURITY CLASSIFICATION OF THIS PAGE (When Data Entered)

REPORT DOCUMENTATION PAGE		READ INSTRUCTIONS BEFORE COMPLETING FORM
1. REPORT NUMBER AFOSR - TR - 74 - 1695	2. GOVT ACCESSION NO.	3. RECIPIENT'S CATALOG NUMBER
4. TITLE (and Subtitle) NEAR FIELD SMALL EARTHQUAKE LONG PERIOD ARRAY		5. TYPE OF REPORT & PERIOD COVERED Interim
		6. PERFORMING ORG. REPORT NUMBER
7. AUTHOR(s) Charles B. Archambeau Donald V. Helmberger		8. CONTRACT OR GRANT NUMBER(s) F44620-72-C-0083
9. PERFORMING ORGANIZATION NAME AND ADDRESS California Institute of Technology Division of Geological & Planetary Sciences Pasadena, CA 91109		10. PROGRAM ELEMENT, PROJECT, TASK AREA & WORK UNIT NUMBERS 62701E A02134
11. CONTROLLING OFFICE NAME AND ADDRESS Advanced Research Projects Agency / NMR 1400 Wilson Boulevard Arlington, VA 22209		12. REPORT DATE 31 May 1974 13. NUMBER OF PAGES 37
14. MONITORING AGENCY NAME & ADDRESS (if different from Controlling Office) Air Force Office of Scientific Research/NP 1400 Wilson Boulevard Arlington, VA 22209		15. SECURITY CLASS. (of this report) UNCL/UNCL 15a. DECLASSIFICATION/DOWNGRADING SCHEDULE

16. DISTRIBUTION STATEMENT (of this Report)

Approved for public release; distribution unlimited

17. DISTRIBUTION STATEMENT (of the abstract entered in Block 20, if different from Report)

18. SUPPLEMENTARY NOTES

19. KEY WORDS (Continue on reverse side if necessary and identify by block number)

20. ABSTRACT (Continue on reverse side if necessary and identify by block number)

This report describes some of the accomplishments achieved during the second year of our cooperative program concerning the detailed nature of seismic radiation from earthquakes. Our efforts have been divided into three areas, to obtain broad-band observations in the Bear Valley region, to develop the theoretical framework needed to treat seismic data in general, and thirdly, to use this formalism to model earthquakes. This year's semi-annual report contains a theoretical treatment of modeling local earthquakes as shear dislocations in a layered halfspace. Numerous synthetic seismograms were presented along with some

DD FORM 1 JAN 73 1473 EDITION OF 1 NOV 65 IS OBSOLETE

UNCLASSIFIED

SECURITY CLASSIFICATION OF THIS PAGE (When Data Entered)

preliminary fits to observations involving strike-slip events. This report presents a generalization of the technique to arbitrary oriented dislocations. The method is used to produce synthetic seismograms at long period P, SV, and SH waveforms at teleseismic distances for various source parameters. Since free surface interaction is different for the various types of waves, one can use this information to refine fault orientation and determine the duration and distribution of the faulting motion. The procedure is presently being used in direct inversion of the observations from the Borrego Mountain earthquake and will be used, shortly, on the San Fernando data.

TABLE OF CONTENTS

ABSTRACT

This report describes some of the accomplishments achieved during the second year of our cooperative program concerning the detailed nature of seismic radiation from earthquakes. Our efforts have been divided into three areas to obtain broad-band observations in the Bear Valley region, to develop the theoretical framework needed to treat seismic data in general, and thirdly, to use this formalism to model earthquakes.

This years semi-annual report contains a theoretical treatment of modeling local earthquakes as shear dislocations in a layered halfspace. Numerous synthetic seismograms were presented along with some preliminary fits to observations involving strike-slip events. This report presents a generalization of the technique to arbitrary oriented dislocations. The method is used to produce synthetic seismograms at long period P, SV, and SH waveforms at teleseismic distances for various source parameters. Since free surface interaction is different for the various types of waves, one can use this information to refine fault orientation and determine the duration and distribution of the faulting motion. The procedure is presently being used in direct inversion of the observations from the Borrego Mountain earthquake and will be used, shortly, on the San Fernando data.

I. Introduction

To put this years effort in proper perspective it seems worthwhile to briefly review previous studies and indicate the direction in which we think our research is evolving. During the first year of this contract we spent most of our efforts in theoretical development (see last years annual report). In particular, the near and far field radiation from relaxation models were extended and generalized for a variety of source geometries and prestress conditions. It was determined that as R_s, the prestress radius, increases to infinity one produced results that were essentially equivalent to Brune's, namely that the spectra is flat for frequencies smaller than the corner frequency. For finite values of R_s, one obtained a peak near the corner frequency that is controlled by the details of the rupture properties, or there is some interaction between the fault dimension and the prestress dimension. These results which are directly attributed to Archambeau further suggest that the corner frequency for P waves can be somewhat higher than for S waves depending on rupture characteristics. Hanks and Wyss (1972) and others have analyzed spectra from a number of shallow earthquakes and indicate that the spectral corner frequency of P waves are significantly higher than that of S waves but this result has been disputed by Helmberger (1974). However, more work is required to answer the corner frequency question as well as relating the fault time history to fault dimension. Shallow moderate sized earthquakes are particularly interesting with regard to these questions since ground breakage can be used to estimate fault dimension. Furthermore, observations from such events provide good measurements of M_s, m_b, and produce long period WWSSN waveform

characteristics as well as local strong motions, this is especially true with respect to the San Fernando earthquake.

To compare observations with synthetics continuously from the local field to teleseismic distances requires considerable effort. This report will be concerned with this problem, namely the presentation of a general technique of modeling shallow dislocation sources imbedded in a layered elastic medium. Much of this material will be published in a paper by Langston and Helmberger, shortly.

II. Theory and Assumptions

In this section, we will cover the model assumptions and the full expressions for an arbitrarily oriented point dislocation in a layered medium.

The first and commonly held assumption is that shallow earthquakes, epicentral depths less than 100 km, are caused by movements along faults, very thin planar zones of weakness. Using this precept, we can specify the entire problem of calculating elastic displacements from this kind of source by use of a finite continuous displacement dislocation in a homogeneous elastic medium. By use of the Green's function solution or representation theorem for movements at a closed surface in an infinite elastic space, one can avoid the problem, somewhat, of non-linear processes at the fault. By placing this surface around the fault zone and saying that each side "knows" what the other is doing (continuity of stress), including a particular fault surface geometry, one can construct the solution for displacements everywhere in the medium given the displacements on the hypothetical surface around the fault. In practice, and mathematically, we assume this surface is very close to the fault and reflects exactly what the real movements are along the fault. This, of course, must be borne out eventually by observations on source finiteness.

Following De Hoop's (1958) form of the elastodynamic representation theorem Harkrider (1974) has produced displacement potentials for a rectangular point shear dislocation in an infinite elastic medium. In terms of the wave number, k, and circular frequency, ω, for an arbitrarily oriented dislocation with the coordinate system of figure 1, these are:

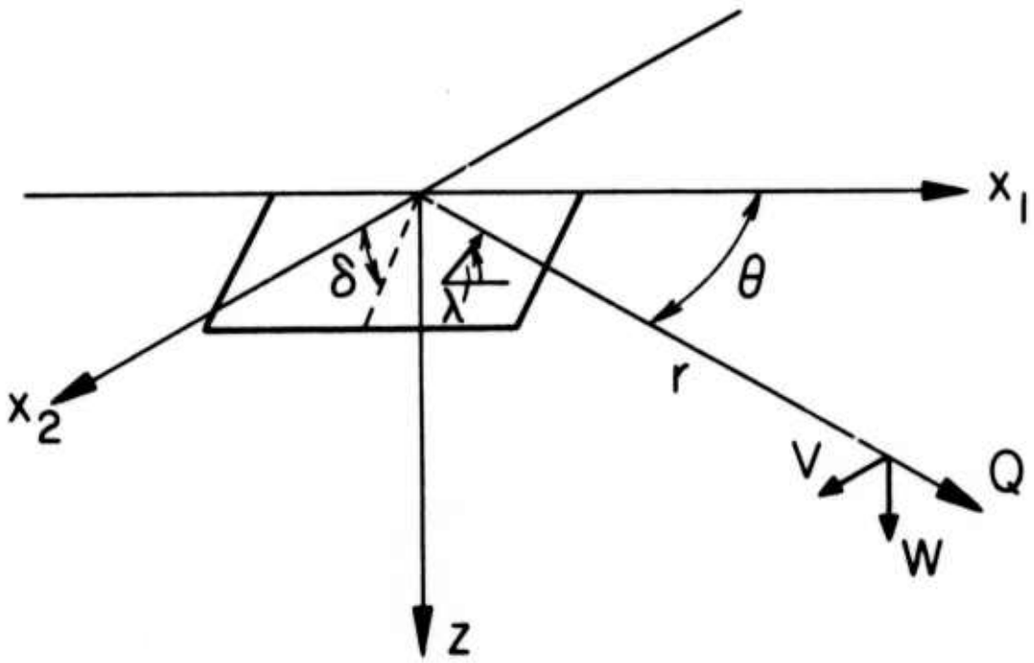

Figure 1. Coordinate system for the dislocation formulation. z is positive downwards.

P Potential

$$\bar{\phi} = -K\int_0^\infty k^2 F_\alpha J_2(kr)dk \cdot A_1(\theta,\lambda,\delta) + K\int_0^\infty 2k\epsilon F_\alpha \nu_\alpha J_1(kr)dk \cdot A_2(\theta,\lambda,\delta) + K\int_0^\infty (2k_\alpha^2 - 3k^2) F_\alpha J_o(kr)dk \cdot A_3(\theta,\lambda,\delta)$$

SV Potential

$$\bar{\Psi} = -K\int_0^\infty \epsilon\nu_\beta F_\beta J_2(kr)dk \cdot A_1(\theta,\lambda,\delta) - K\int_0^\infty \frac{(k_\beta^2 - 2k)}{k} F_\beta J_1(kr)dk \cdot A_2(\theta,\lambda,\delta) - K\int_0^\infty 3\epsilon F_\beta \nu_\beta J_o(kr)dk \cdot A_3(\theta,\lambda,\delta) \quad (1)$$

SH Potential

$$\bar{\chi} = +K\int_0^\infty k_\beta^2 F_\beta J_2(kr)dk \cdot A_4(\theta,\lambda,\delta) - K\int_0^\infty \frac{k_\beta^2}{k} \epsilon F_\beta \nu_\beta J_1(kr)dk \cdot A_5(\theta,\lambda,\delta)$$

where,

α = compressional wave velocity

β = shear wave velocity

$k_v = \omega/v$

$$\nu_v = (k^2 - k_v^2)^{1/2}$$

$$F_v = \frac{ke^{-\nu_v|z - h|}}{\nu_v}$$

h = depth to source

$$K = -\frac{\mu L H \bar{D}(\omega)}{4\pi\rho\omega^2}$$

μ = shear modulus at the source

ρ = density at the source

$$\varepsilon = \begin{cases} +1 & z > h \\ -1 & z < h \end{cases}$$

L = fault length

H = fault height

$\bar{D}(\omega)$ = transformed dislocation time function

$$A_1(\theta,\lambda,\delta) = \sin 2\theta \cos\lambda \sin\delta + \frac{1}{2}\cos 2\theta \sin\lambda \sin 2\delta$$

$$A_2(\theta,\lambda,\delta) = \cos\theta \cos\lambda \cos\delta - \sin\theta \sin\lambda \cos 2\delta$$

$$A_3(\theta,\lambda,\delta) = \frac{1}{2}\sin\lambda \sin 2\delta \qquad (2)$$

$$A_4(\theta,\lambda,\delta) = \cos 2\theta \cos\lambda \sin\delta - \frac{1}{2}\sin 2\theta \sin\lambda \sin 2\delta$$

$$A_5(\theta,\lambda,\delta) = -\sin\theta \cos\lambda \cos\delta - \cos\theta \sin\lambda \cos 2\delta$$

θ = strike from the end of the fault plane

λ = rake angle

δ = dip angle

The displacements in the medium are given by:

$$\bar{W}(r,z,\theta,\omega) = \frac{\partial \bar{\phi}}{\partial z} + \frac{\partial^2 \bar{\psi}}{\partial z^2} + k_\beta^2 \bar{\psi}$$

$$\bar{V}(r,z,\theta,\omega) = \frac{1}{r}\frac{\partial \bar{\phi}}{\partial \theta} + \frac{1}{r}\frac{\partial^2 \bar{\psi}}{\partial z \partial \theta} - \frac{\partial \bar{\chi}}{\partial r} \qquad (3)$$

$$\bar{Q}(r,z,\theta,\omega) = \frac{\partial \bar{\phi}}{\partial r} + \frac{\partial^2 \bar{\psi}}{\partial r \partial z} + \frac{1}{r}\frac{\partial \bar{\chi}}{\partial \theta}$$

The first, second, and third terms of the P-wave and SV-wave potentials, excluding the angle terms, A_i , correspond to a vertical strike-slip dislocation, a vertical dip-slip dislocation, and a dislocation dipping at 45° seen at 45° azimuth, respectively. The SH potential contains the vertical strike-slip and vertical dip-slip dislocations, respectively. This order will be kept throughout the paper.

Changing variables into a form more convenient for generalized ray theory, that is, k into p , the ray parameter, and ω into s , the Laplace Transform variable, we obtain:

<u>P-waves</u>

$$\hat{\phi} = -\frac{M_o}{4\pi\rho}\frac{2}{\pi}\,\mathrm{Im}\int_o^{+i\infty} \frac{p^3}{\eta_\alpha} e^{-s\eta_\alpha|z-h|} K_2(spr)dp \cdot A_1(\theta,\lambda,\delta)$$

$$+ \frac{M_o}{4\pi\rho}\frac{4}{\pi}\,\epsilon\,\mathrm{Im}\int_o^{+i\infty} p^2 e^{-s\eta_\alpha|z-h|} K_1(spr)dp \cdot A_2(\theta,\lambda,\delta)$$

$$- \frac{M_o}{4\pi\rho}\frac{2}{\pi}\,\mathrm{Im}\int_o^{+i\infty} \left(\frac{2}{\alpha^2} - 3p^2\right)\frac{p}{\eta_\alpha} e^{-s\eta_\alpha|z-h|} K_o(spr)dp \cdot A_3(\theta,\lambda,\delta)$$

SV-waves

$$\hat{\Omega} = -\frac{M_o}{4\pi\rho}\frac{2}{\pi}\,\varepsilon\,\mathrm{Im}\int_o^{+i\infty} p^2 e^{-s\eta_\beta|z-h|} K_2(spr)dp \cdot A_1(\theta,\lambda,\delta)$$

$$-\frac{M_o}{4\pi\rho}\frac{2}{\pi}\,\mathrm{Im}\int_o^{+i\infty} \frac{\left(2p^2-\frac{1}{\beta^2}\right)}{\eta_\beta} pe^{-s\eta_\beta|z-h|} K_1(spr)dp \cdot A_2 \qquad (4)$$

$$+\frac{M_o}{4\pi\rho}\frac{6}{\pi}\,\varepsilon\,\mathrm{Im}\int_o^{+i\infty} p^2 e^{-s\eta_\beta|z-h|} K_o(spr)dp \cdot A_3$$

SH-waves

$$\hat{\chi} = +\frac{M_o}{4\pi\rho}\frac{2}{\pi}\frac{1}{\beta^2}\,\mathrm{Im}\int_o^{+i\infty} \frac{p}{\eta_\beta} e^{-s\eta_\beta|z-h|} K_2(spr)dp \cdot A_4$$

$$-\frac{M_o}{4\pi\rho}\frac{2}{\pi}\frac{\varepsilon}{\beta^2}\,\mathrm{Im}\int_o^{+i\infty} e^{-s\eta_\beta|z-h|} K_1(spr)dp \cdot A_5$$

where the following transformations have been made,

$\omega = -is$

$k = -isp$

$\hat{\Omega} = -sp\hat{\psi}$, SV potential transformation

$M_o = LHD_o\mu$, fault moment

$\hat{D}(s) = \frac{D_o}{S}$, a step function weighted by D_o

$\eta_v = \left(\frac{1}{v^2} - p^2\right)^{\frac{1}{2}}$

$\hat{}$ = Laplace transformed

The nature of the variable changes and SV potential transformation is discussed in Helmberger (1974). The displacements after these transformations are:

$$\hat{W} = \frac{\partial \hat{\phi}}{\partial z} + sp\hat{\Omega}$$

$$\hat{V} = \frac{1}{r}\frac{\partial \hat{\phi}}{\partial \theta} - \frac{1}{spr}\frac{\partial^2 \hat{\Omega}}{\partial z \partial \theta} - \frac{\partial \hat{\chi}}{\partial r} \qquad (5)$$

$$\hat{Q} = \frac{\partial \hat{\phi}}{\partial r} - \frac{1}{sp}\frac{\partial^2 \hat{\Omega}}{\partial r \partial z} + \frac{1}{r}\frac{\partial \hat{\chi}}{\partial \theta}$$

The potential forms (4) are well suited in calculations involving layered structure since one just multiplies the appropriate generalized reflection coefficients into the integrals before evaluation. Our expressions can be further simplified by using the asymptotic expansion for the modified Bessel functions.

We have:

$$\hat{\phi} = \frac{M_o}{4\pi\rho}\sum_{j=1}^{3} A_j(\theta,\lambda,\delta)\frac{2}{\pi}\,\mathrm{Im}\int_o^{+i\infty} C_j \frac{p}{\eta_\alpha}\sqrt{\frac{\pi}{2spr}}\, e^{-s(pr + \eta_\alpha|z-h|)}\,dp$$

$$\hat{\Omega} = \frac{M_o}{4\pi\rho}\sum_{j=1}^{3} A_j(\theta,\lambda,\delta)\frac{2}{\pi}\,\mathrm{Im}\int_o^{+i\infty} SV_j \frac{p}{\eta_\beta}\sqrt{\frac{\pi}{2spr}}\, e^{-s(pr + \eta_\beta|z-h|)}\,dp \qquad (6)$$

$$\hat{\chi} = \frac{M_o}{4\pi\rho}\sum_{j=1}^{2} A_{(j+3)}(\theta,\lambda,\delta)\frac{2}{\pi}\,\mathrm{Im}\int_o^{+i\infty} SH_j \frac{p}{\eta_\beta}\sqrt{\frac{\pi}{2spr}}\, e^{-s(pr + \eta_\beta|z-h|)}\,dp$$

where

$$C_1 = -p^2 \qquad SV_1 = -\varepsilon p \eta_\beta \qquad SH_1 = \frac{1}{\beta^2} \qquad (7)$$

$$C_2 = 2\varepsilon p \eta_\alpha \qquad SV_2 = (\eta_\beta^2 - p^2) \qquad SH_2 = -\frac{\varepsilon}{\beta^2}\frac{\eta_\beta}{p}$$

$$C_3 = (p^2 - 2\eta_\alpha^2) \qquad SV_3 = 3\varepsilon p\eta_\beta$$

One final form which is useful is the first motion approximations. This approximation supposes that the above functions can be taken outside the integral and evaluated at the appropriate ray parameter yielding the standard vertical radiation patterns, see Helmberger (1974). Transforming into the time domain, these forms become:

$$\phi = \frac{M_o}{4\pi\rho} \sum_{j=1}^{3} A_j(\theta,\lambda,\delta)\ C_j \frac{H\left(t - \frac{R}{\alpha}\right)}{R}$$

$$\Omega = \frac{M_o}{4\pi\rho} \sum_{j=1}^{3} A_j(\theta,\lambda,\delta)\ SV_j \frac{H\left(t - \frac{R}{\beta}\right)}{R} \qquad (8)$$

$$\chi = \frac{M_o}{4\pi\rho} \sum_{j=1}^{2} A_{j+3}(\theta,\lambda,\delta) SH_j \frac{H\left(t - \frac{R}{\beta}\right)}{R}$$

where,

$H\left(t - \frac{R}{V}\right)$ = step function delayed by travel time $\frac{R}{\beta}$

R = distance the ray travels

The far-field displacements become:

$$W = \eta_\alpha \dot{\phi} + p\dot{\Omega}$$

$$Q = -p\dot{\phi} + \eta_\beta \dot{\Omega} \qquad (9)$$

$$V = p\dot{\chi}$$

where the dot indicates the derivative with respect to time. These results are useful for wave calculations when the signal duration is short compared to the travel time and will be used extensively in the remaining sections

of this paper.

One other point should be mentioned on the use of these potentials. Earthquakes obviously are not point sources so why or with what justification can one use this representation? The answer to this is simple. Because the problem as posed is linear, the principle of superposition can be applied. The idea is that a series of spatially and temporally separated point dislocations can be summed to approximate a heterogeneous slipping fault surface. Since it is very cumbersome, if not impossible, to put in the effects of earth structure directly with a finite sized fault, this approach of taking infinitesimal faults, computing the structure effect through propagating potentials, and then summing each individual fault contribution makes for a much swifter, efficient, and tractable operation.

a. Shallow Source Modeling: 30-90°

Ben-Menshem, Smith, and Teng (1965) have given a very thorough discussion of the procedures used for body-wave analysis of deep and intermediate depth earthquakes. Essentially, the methods outlined here are very similar except for the important and justifying difference of including the earth structure effect through the use of potentials and reflection-transmission coefficients.

We introduce our technique of categorizing the various effects by means of a representative calculation.

Consider the problem setup displayed in figure 2 where the goal is to produce a P-wave synthetic seismogram at the receiver for the rays shown. The total vertical response at the receiver can be given

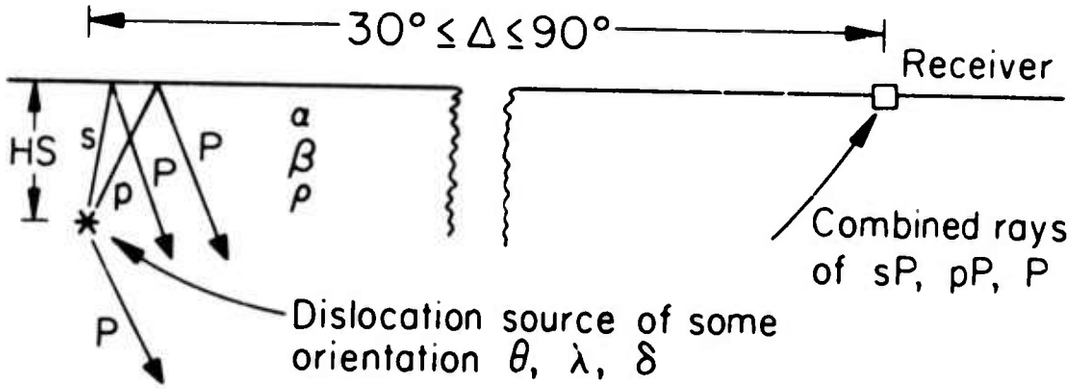

Figure 2. Schematic representation of equation (10).

by the following equation:

$$W = + \eta_\alpha R_{PZ}[\dot{\phi} + R_{PP}\dot{\phi} \cdot H(t - \Delta t_1) + R_{SP}\dot{\Omega} \cdot H(t - \Delta t_2)] * S(t) * I(t) * Q(t) \quad (10)$$

where,

R_{PZ} = vertical P-wave receiver function

R_{PP} = reflection coefficient for pP

R_{SP} = reflection coefficient for sP

$S(t)$ = far-field dislocation time function

$I(t)$ = impulse response of an instrument

$Q(t)$ = Q operator

$*$ = convolution operator

Δt_1 = time lag of pP relative to the direct wave

Δt_2 = time lag of sP relative to the direct wave

$H(t - \Delta t)$ = lagged Heaviside step function

Remember that z is positive downward. Note also that the SV potential, Ω, appears in this P-wave calculation since it must serve as an amplitude weighting function for the ray sP. In practice, for these ranges, one ray parameter is used for all near source interactions. For shallow sources the error introduced by this approximation is negligible. For the same ray parameter then, we have the time lags given simply as

$$\Delta t_1 = 2HS\eta_\alpha \tag{11}$$

$$\Delta t_2 = HS\,(\eta_\beta + \eta_\alpha) \quad .$$

The far-field time function, $S(t)$, is the derivative of the actual dislocation displacement time function. This comes about by setting $D(s) = \frac{D_o}{s}$ in (4) to get the step-function response of the potentials. The impulse response, which is needed for the convolution operations, is simply the time derivative. For convenience, and by superposition, we do this derivative on the displacement time function to give the far-field time function. Also, since we weighted the step-function response by D_o, the final offset, we must set the final offset of each displacement time function used to be 1. Denoting the displacement time function by $f(t)$, this corresponds to:

$$\int_{-\infty}^{+\infty} \frac{\partial f(t)}{\partial t}\, dt \equiv \int_{-\infty}^{+\infty} S(t)dt \equiv 1 \tag{12}$$

The fault moment, M_o, contained in the potentials (4), (7), and (8), is taken to be expressed in the conventional units of ergs (dyne-cm) and density, ρ, in gm/cm^3.

The instrument response, I(t), is usually normalized to one of its particular frequency components. For example, using Hagiwara's (1958) equations, one can construct the instrument response for the 15-100 WWSSN long period instrument, such that the amplitude of the 15 second period spectral component is equal to unity. This form is used in all the synthetic seismogram calculations of this paper.

The reflection and transmission coefficients are those used by

Helmberger (1968) and, in this case, are simple multiplicative constants. If evaluated inside the integrals (7) or (4), as the general case, a range of complex ray parameters defined by the Cagniard contour is used.

The receiver functions R_{PZ}, R_{PR}, R_{SZ} and R_{SR} are explicitly given in Helmberger (1974) and behave as simple real functions of p over the ranges considered. The letter index of this notation tells the wave type and receiver component, respectively. A fifth receiver function defined by $R_T = (2p)$ describing the tangential displacement at the free surface is added for completeness, see expression (5). Table 1 shows the variations expected in these functions for different receiver crust models and ranges. The table is made with z positive upwards. As can be seen, these functions are fairly slow varying over these ranges.

Futterman's Q operator (1962) using a constant T/Q ratio will be the basis for the Q(t) term in all calculations. It has the property of preserving pulse area so no scaling problems arise from using it.

The expressions for the potentials were derived for a homogeneous earth with the spreading term (1/R). The effective (1/R) for a real earth is somewhat smaller, see figure 3, and can be approximated by the method used by Helmberger (1973a). The amplitudes were measured directly from the synthetic step function responses generated from an earth-flattened Jeffreys-Bullen model and plotted versus range. This curve is equivalent to a smoothed geometrical optics calculation and contains some theoretical uncertainty as pointed out by Chapman (1974). There is also the problem of earth structure uncertainty which could easily produce significant waveshape distortions. We will neglect these interesting problems here and concentrate on waveshapes produced by the source and accompanying surface reflections.

Table 1. Evaluation of the receivers functions for various ray parameters and crustal models.

Crust Model	$\Delta^{(o)}$	p (P-waves)	p (S-waves)	R_{PZ}	R_{PR}	R_{SZ}	R_{SR}	R_T
α = 6.0	90°	.040	.069	-0.321	-0.093	-.158	.545	.138
β = 3.5	60°	.060	.104	-0.306	-0.138	-.231	.511	.208
	30°	.080	.139	-0.285	-0.182	-.288	.484	.278
α = 5.5	90°	.040	.069	-0.353	-0.093	-.158	.600	.138
β = 3.2	60°	.060	.104	-0.339	-0.138	-.232	.570	.208
	30°	.080	.139	-0.320	-0.182	-.296	.536	.278
α = 5.0	90°	.040	.069	-0.390	-0.092	-.158	.667	.138
β = 2.9	60°	.060	.104	-0.378	-0.138	-.234	.640	.208
	30°	.080	.139	-0.360	-0.182	-.301	.605	.278

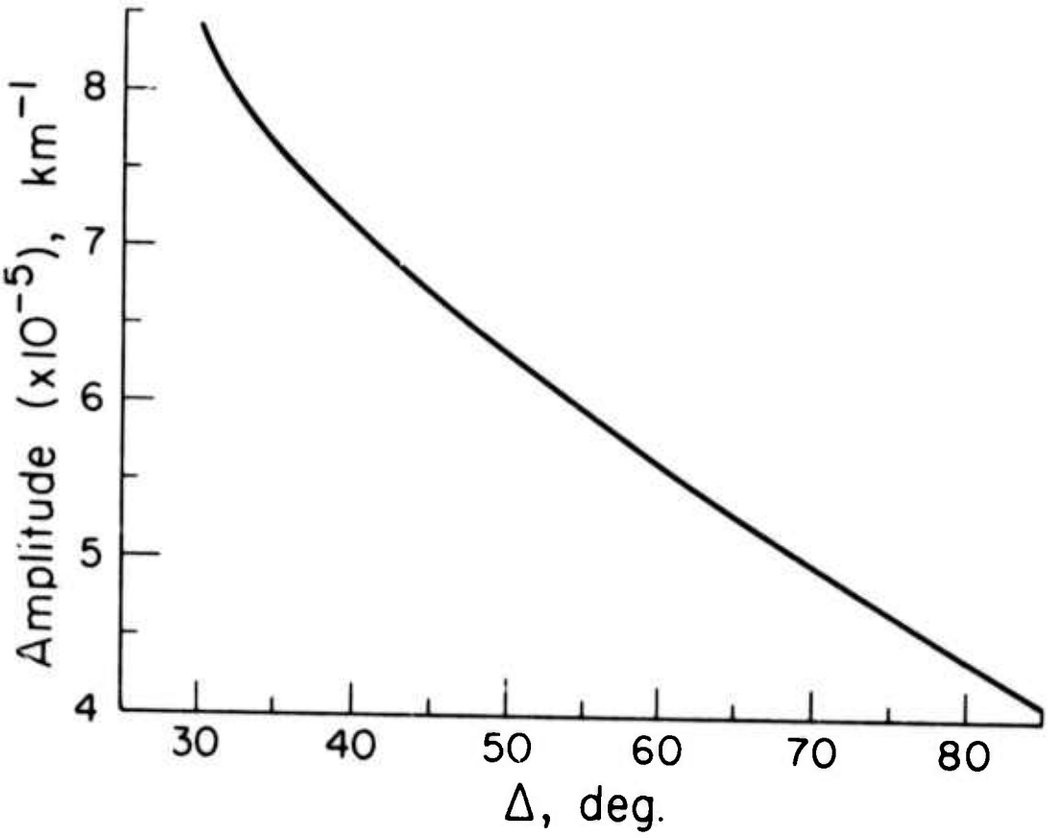

Figure 3. Graph of the effective 1/R decay in a Jeffreys-Bullen spherical earth.

b. Source Time Function Scaling

Making certain assumptions about the seismic source one can derive scaling laws for the source time function which include parameters such such as stress-drop, fault moment, and corner frequencies, see Brune (1970). The basic relationship is that the ratio of fault displacement, D_o, to fault dimension, r, is proportional to the ratio of stress drop, σ, to μ, the rigidity. We can derive Brune's results rather easily from shear dislocation theory. Starting with the SH potential, χ, of equation (8), assuming a vertical strike-slip fault ($\delta = 90°$, $\lambda = 0°$), and taking the necessary derivative indicated by (9) we get for the far-field tangential displacement

$$\upsilon = \frac{M_o}{4\pi\rho} \frac{1}{\beta^3} R_{\phi\theta} \frac{\delta\left(t - \frac{R}{\beta}\right)}{R} \tag{13}$$

where we have set $R_{\phi\theta} = \sin\phi \cos 2\theta$, the radiation pattern. The $\sin\phi$ term comes from the relation $p = \sin\phi/\beta$, where ϕ is the take-off angle from vertical. Assuming the far-field time history discussed above, we have

$$\upsilon = \frac{M_o}{4\pi\rho} \frac{1}{\beta^3} R_{\phi\theta} \left(\frac{1}{R}\right) \frac{\partial f\left(t - \frac{R}{\beta}\right)}{\partial t} \tag{14}$$

For an assumed Brune time history, leads to

$$\frac{\partial f}{\partial t} = \alpha^2 t e^{-\alpha t} \tag{15}$$

and assuming a circular fault, Keilis Borok (1960),

$$\upsilon = R_{\phi\theta} \left(\frac{\sigma}{\mu}\right) \beta \left(\frac{r}{R}\right) t \; e^{-\alpha t} \tag{16}$$

by further assuming that

$$\alpha = \frac{\sqrt{7\pi}}{2} \left(\frac{\beta}{r}\right) . \tag{17}$$

The spectrum corresponding to (16) is simply

$$\Omega(\omega,\theta,\phi,R) = R_{\phi\theta} \left(\frac{\sigma}{\mu}\right) \beta \left(\frac{r}{R}\right)\left(\frac{1}{\omega^2 + \alpha^2}\right) \tag{18}$$

which leads to the "corner frequency" phenomenon. Generally speaking then, this model says that the frequency of the time function is inversely proportional to the fault dimension; the longer the fault (or lower the stress-drop) the longer the time function lasts. We will incorporate this idea in a semiquantitative way in the discussion of the synthetic seismograms.

The far-field source time function assumed here will be a trapezoid of unit height described by three time parameters, δt's. The time length of the positive, zero and negative slopes will be represented by δt_1, δt_2, and δt_3, respectively. These three δt's allow relative time scaling of such things as rise time, fault duration, and stopping time. This time function will be normalized by the convention assumed, that is, of equation (12).

c. Synthetic Seismograms

Synthetic seismograms were computed for P, SV, and SH waves for a

point dislocation source in a halfspace using relations (8) after the method described by (10). The halfspace model uses a compressional velocity of 6.0 km/sec, shear velocity of 3.5 km/sec, and density equal to 2.7 gm/cm^3. The distance from the source was taken as 80° which corresponds to a ray parameter of about .05 for P-waves and about .087 for S-waves.

For P-waves a constant $\frac{T}{Q}$ ratio of 1.0 was used in Futterman's Q operator, Helmberger (1973b). For S-waves a conservative estimate of $\frac{T}{Q} = 3.0$ was used.

The impulse response for the 15-100 WWSSN instrument was used in all calculations.

Each of the respective sets of synthetic seismograms, P , SV , and SH of figures 4, 5 and 6 are arrayed with the purpose of showing the contribution and effect of each of the j^{th} terms of equation (8). Each one of these terms (j = 1,2,3) can be given a separate physical interpretation. Not considering the radiation pattern, A_j , j = 1 represents a vertical strike-slip fault, j = 2 a vertical dip-slip fault, and j = 3 a 45° dipping dip-slip fault as seen at 45° azimuth. To produce any other oriented point dislocation, one just multiplies the appropriate A_j for each orthogonal term and sum. This particular orthogonality relationship came originally from the way the Green's function solution grouped together as double-couple representations.

The P waveforms all contain the surface interactions pP and sP as described by equation (10), along with the direct wave. Likewise, by analogous calculations, the SV waveforms contain S , sS and pS and the SH waveforms S and sS . The left-hand side of each diagram contains a representation of the medium impulse response for the source depth

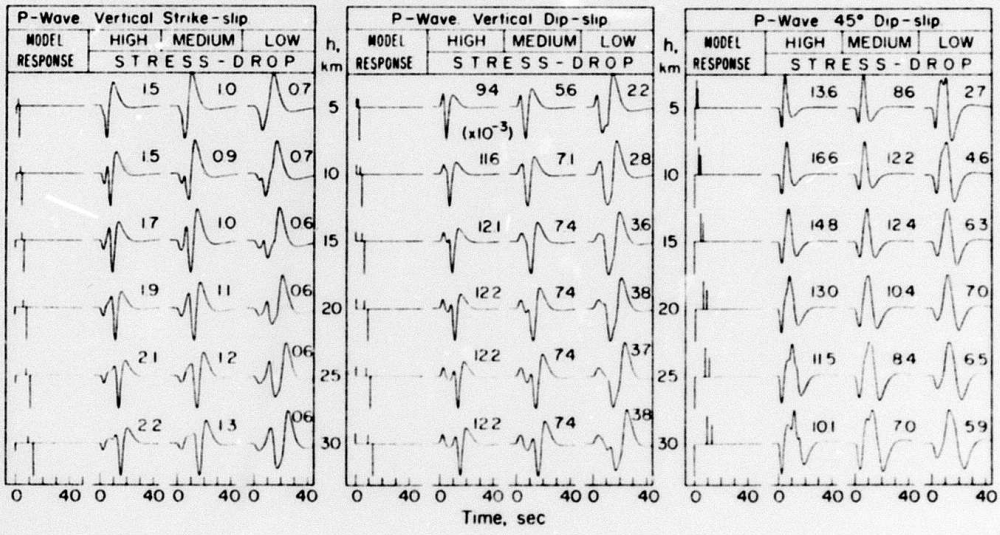

Figure 4. P-wave synthetic seismograms for the three potential terms with varying depth and time functions. The numbers to the upper right are actual potential amplitudes without the moment $1/4\pi\rho$, 1/R decay, and receiver functions included.

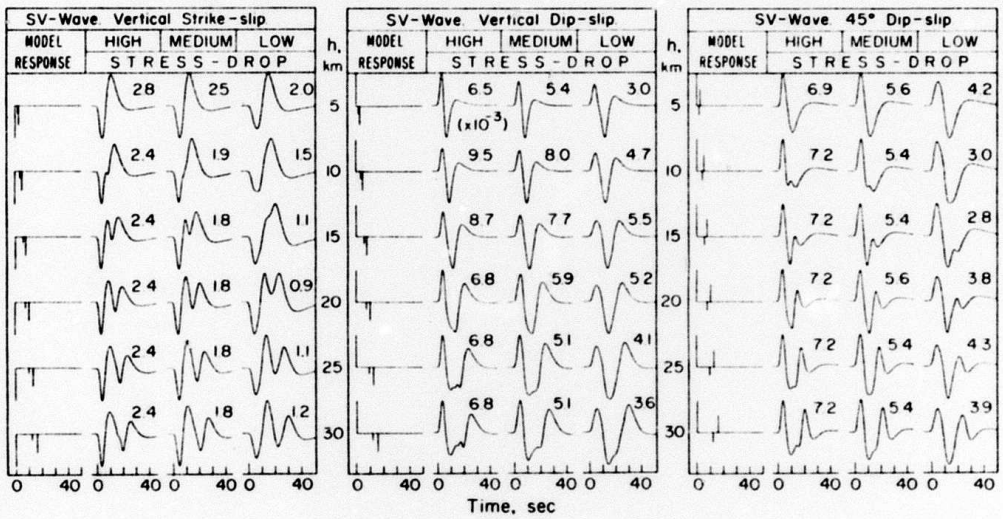

Figure 5. SV-wave synthetic seismograms. Same scheme as Figure 4.

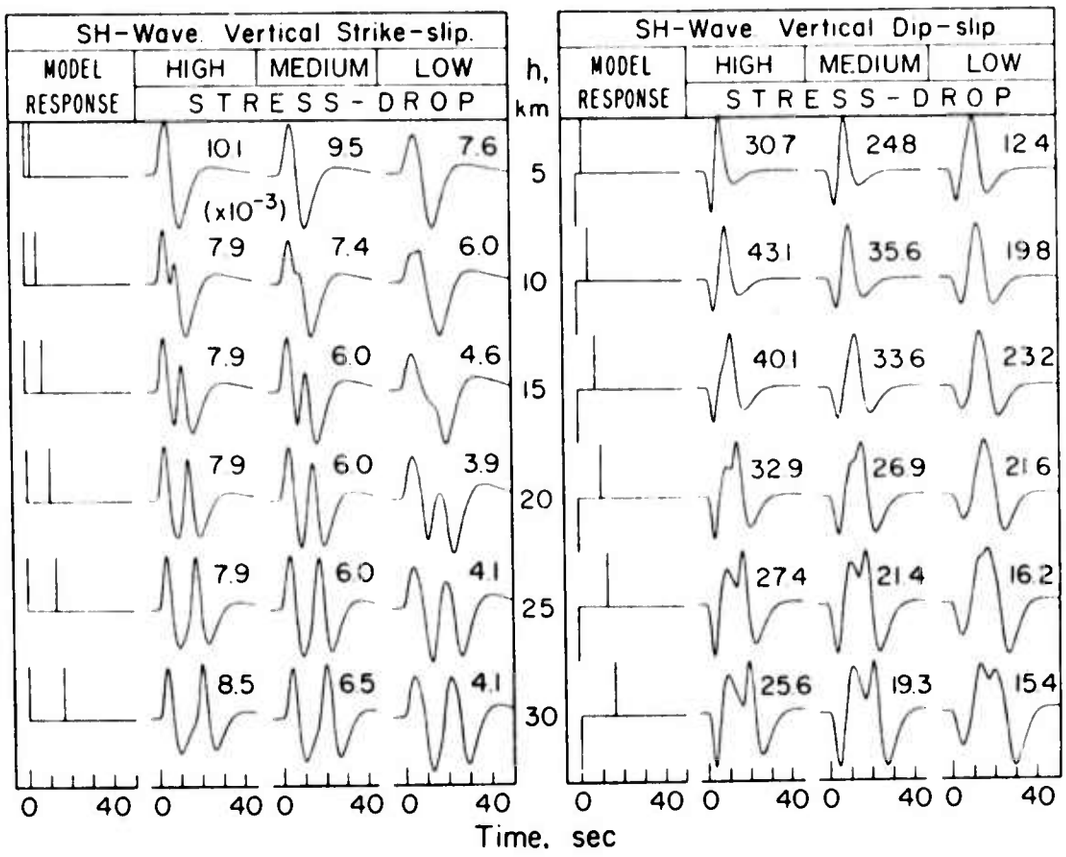

Figure 6. SH-wave synthetic seismograms. Same scheme as Figure 4.

considered. The relative spike height corresponds to the weights of the delta functions. In each column to the right of it are the synthetic seismograms obtained by convolving in the instrument, Q , and the particular source time function considered. The "stress-drop" conotation used here is a very simple one based on the length of the time function as discussed before. Table 2 displays the time function parameters used for the various designated stress-drop calculations.

Even a cursory examination of figures 4 and 5 show that the phases pP , sP and sS are often as large, if not larger, an effect as the direct wave. Compare, for contrast, with figure 7, which displays what the waveform would look like without the surface interactions.

The amplitudes indicated by each synthetic of figures 4, 5 and 6 do not contain the factors of $M_o/4\pi\rho$, $\frac{1}{R}$, the appropriate receiver function, or an instrument magnification. To get the amplitude, one just multiplies in the appropriate constants as discussed and also a unit conversion constant, $\overline{10}^{20}$, for units of centimeters, or $\overline{10}^{16}$, for microns.

Note that polarity of sP in the dip-slip case of figure 5 is different from that of Helmberger (1974) due to a sign error in the SV potential as mentioned earlier.

Figure 8 shows a sample calculation for summing the three orthogonal faults. These synthetics are appropriate for a station at 80° distance and 30° azimuth from a northward striking fault plane of figure 1. The amplitudes are scaled, taking all the factors discussed above into account with a fault moment of $M_o = 10^{25}$ ergs.

Two important observations can be made from this figure. The first, and obvious one, is that the waveforms are complicated due to the surface

Table 2

Source Time Function Parameters

	high stress-drop	medium stress-drop	low stress-drop
δt_1	0.5	1.0	2.0
δt_2	1.5	3.0	6.0
δt_3	0.5	1.0	2.0

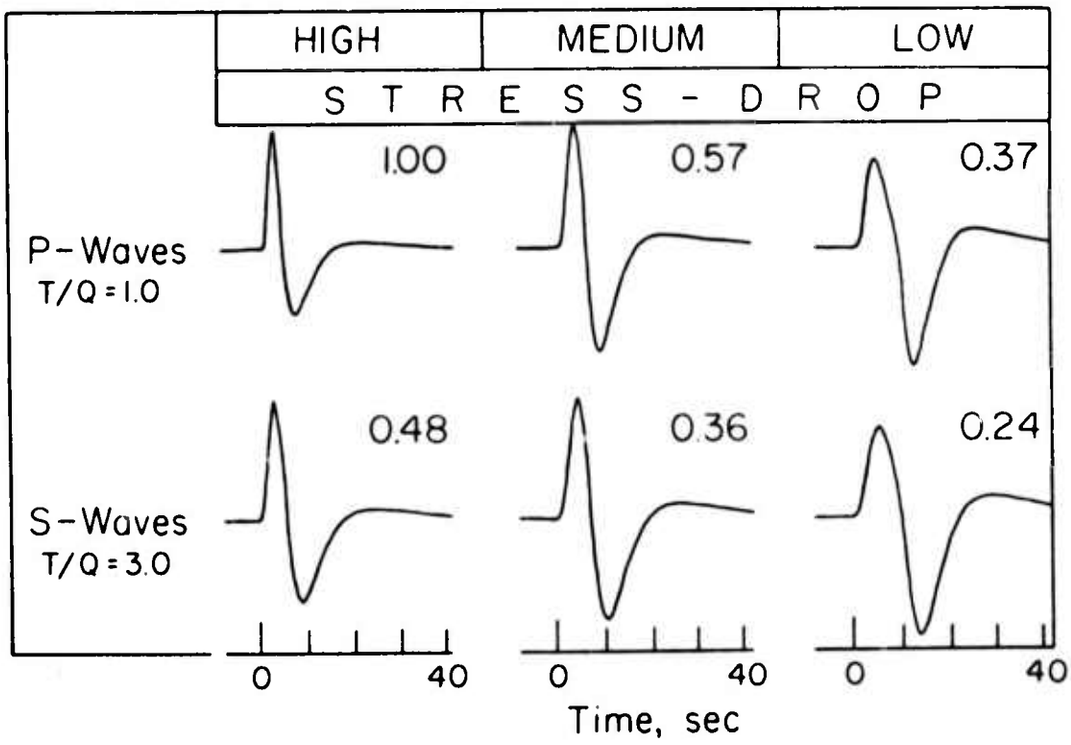

Figure 7. Synthetics of the time function indicated convolved with the 15-100 instrument with no crustal interactions. Amplitudes scaled to the high stress-drop P-wave.

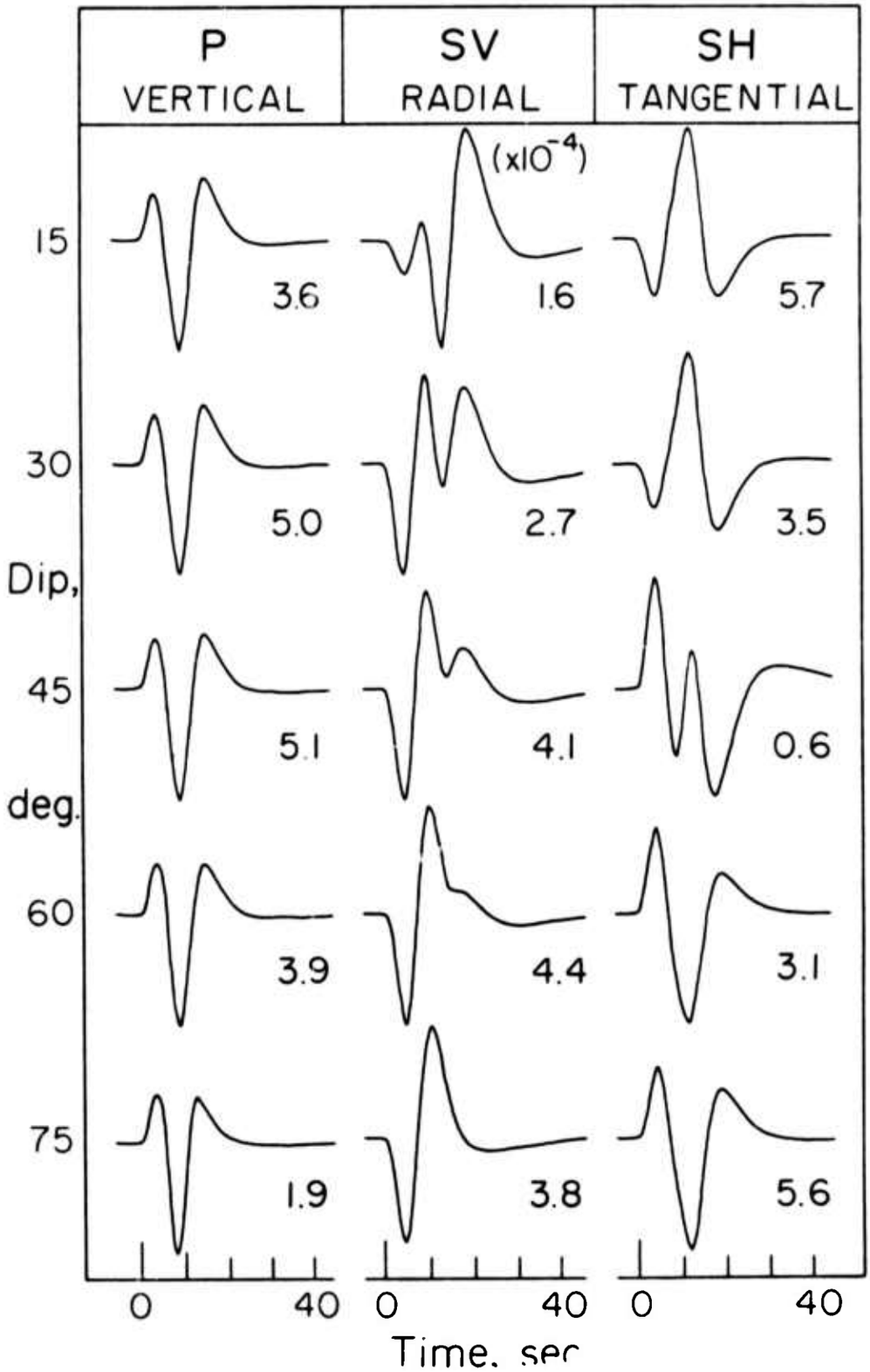

Figure 8. Synthetics of P, SV, and SH waves from a 15 km deep medium stress-drop dislocation with a moment of 10^{25} ergs seen at 30° azimuth, 80° distance, for various fault plane dips. The rake angle for all dips is 90° representing a thrust fault. Amplitudes are in cm. Positive P starts as a compression, positive SV is motion away from the source, and positive SH is clockwise motion looking from above.

interactions. They do not look like figure 7. The second is that, due to the increased relative travel time between S and sS as opposed to P and pP and also the increased $\frac{T}{Q}$ for S-waves, the S-waves appear to be longer period than the P-waves. A number of recent investigators have suggested the S-waves corner frequency to be at longer periods than that of the P-waves. Here is a simple mechanism of producing such an effect with a simple shear dislocation without recourse to more complicated source mechanisms.

III. Discussion

The use of the potentials and methods presented here provides a useful tool for the study and modeling of shallow earthquakes. By separating the reflected phases from the direct arrivals, one can gain a clearer picture of the source mechanism and, hopefully, a better appreciation of the processes that produce earthquakes.

An interesting feature of this method of waveform analysis is that for earthquakes with relatively simple time functions the information contained in a seismogram increases dramatically for use in focal mechanisms. Each of the phases pP , sP , sS , and pS contain just as much information about the source as do the direct waves. By recognizing these phases, the seismogram can be put to much better use than has been previously possible. For example, it is theoretically possible, in many

cases of fault-plane orientations, to find a well-constrained fault plane solution using very few stations by modeling the P and S waveforms and relative amplitudes.

This approach of seismic modeling using point sources will also be very useful in the near-field. Using generalized ray theory layered earth structure can be incorporated into fault models composed of catenated arrays of point sources. This will allow realistic earthquake strong-motion calculations.

These subjects will be the basis for future work in earthquake source modeling. Abstracts of two such studies are given below.

The Relationship Between Teleseismic P-Wave and Near-Field Strong Motion Observations for the February 9, 1971, San Fernando Earthquake, by Charles A. Langston

Long-period P-waves from 17 azimuthally varying WWSSN stations reveal dinstinctive source complications during the San Fernando earthquake. Preliminary results show that the teleseimic record is dominated by crustal phase interactions from two different source areas on the San Fernando fault plane. Represented by two point dislocation sources of nearly equal moment, one at about 14 km depth with the fault plane parameters of Whitcomb et al. (1973), and the other at about 4 km depth with about 10° less dip, synthetic seismograms are calculated through the use of potential ray theory and compare very well with the teleseismic observations. Using the Cagniard-de Hoop method near-field SH displacement synthetic seismograms are constructed for this model and are favorably compared with Hanks' (1974) profile 1 of twice integrated accelerograms.

Determination of Source Parameters from Body Wave Seismograms, by G. R. Mellman, L. J. Burdick, and D. V. Helmberger

A method of obtaining fault parameters from long period body wave seismograms has been developed. Using inversion techniques to simultaneously fit waveforms of seismograms recorded at a number of stations at teleseismic distances, fault orientation parameters and duration of the source time function may be determined. For multiple events, multiple fault orientations and multiple time functions may be obtained. Studies of synthetic problems indicate that this method may be used to refine fault plane solutions where inadequate first motion data are present, to obtain far field time functions for shallow events, and to do resolution studies on fault parameters. These techniques are applied to determine a far field time function for the Borrego Mountain earthquake.

References

Ben-Menahem, A., S.W. Smith, and T.L. Teng (1965). A procedure for source studies from spectra of long-period seismic waves, Bull. Seism. Soc. Am., 55, 203-255.

Brune, J.N. (1970). Tectonic stress and the spectra of seismic waves from earthquakes, J. Geophys. Res., 75, 4997-5009.

Chapman, C.H. (1974). Generalized ray theory for an inhomogeneous medium, Geophys. J. R. Astr. Soc., 36, 673-704.

De Hoop, A.T. (1958). Representation theorems for the displacement in an elastic solid and their application to elastodynamic diffraction theory. Thesis, Technische Hogeschool, Delft.

Futterman, W.I. (1962). Dispersive body waves, J. Geophys. Res., 67, 5279-5291.

Hagiwara, T. (1958). A note on the theory of the electromagnetic seismograph, Bull. Earthquake Res. Inst., 36, 139-164.

Harkrider, D.G. (1973). Potential representations of a point source dislocation (in preparation).

Helmberger, D.V. (1968). The crust-mantle transition in the Bering Sea, Bull. Seism. Soc. Am., 58, 179-214.

Helmberger, D.V. (1973a). Numerical seismograms of long-period body waves, from seventeen to forty degrees, Bull. Seism. Soc. Am., 63, 633-646.

Helmberger, D.V. (1973b). On the structure of the low-velocity zone, Geophys. J. R. Astr. Soc., 34, 251-263.

Helmberger, D.V. (1974). Generalized ray theory for shear dislocations, Bull. Seism. Soc. Am., 64, 45-64.

Keilis-Borok, V.I. (1960). Investigation of the mechanism of earthquakes, Sov. Res. Geophys., 4, 29.